A Three-Dimensional Two-Energy-Group Finite-Difference Neutron-Diffusion Code With Discontinuity Factors

E. Nichita, K. Zabienski and M. Gravel

University of Ontario Institute of Technology, Oshawa, Ontario, Canada

Abstract

Full-core neutronic calculations are usually carried out in diffusion theory, using fuel-bundle-size homogenized nodes. A simple way to evaluate the neutronic parameters for the homogenized nodes is to calculate flux-weighted fuel-bundle-averaged multigroup macroscopic cross sections. This is known as Standard Homogenization (SH). SH produces satisfactory results for mildly heterogeneous configurations but fails to do so for more heterogeneous ones. To address this issue, advanced homogenization techniques have been developed, such as Superhomogenization (SPH) and Generalized Equivalence Theory (GET). While SPH can be used with any neutron diffusion code without requiring it to be altered, GET requires that some changes be implemented into the numerical formalism employed for the solution of the multigroup diffusion equations, in particular the introduction of *discontinuity factors* at node interfaces. The present work describes the implementation of discontinuity factors into a simple two-energy-group three-dimensional finite-difference diffusion code. Test results for simple configurations are also presented.

1. Introduction

Full-core neutronic calculations are usually carried out in diffusion theory, using fuel-bundle-size homogenized nodes. The detailed geometric core model is called the heterogeneous model, while the simplified, homogeneous-node model is called, simply, the homogeneous model. Likewise, the detailed flux is called the heterogeneous flux, while the flux obtained for the homogeneous model is called the homogeneous flux. The accuracy of the full core calculation depends to a large degree on the method used to generate the neutronic parameters for the homogenized nodes. A simple way to calculate such homogenized parameters is to calculate flux-weighted average multigroup macroscopic cross sections for each node. This is known as Standard Homogenization (SH). SH produces satisfactory results for configurations that do not possess a large degree of heterogeneity such as is the case for natural-uranium fuelled and heavy-water cooled and moderated CANDU cores. For more heterogeneous configurations, such as those encountered in Light Water Reactors (LWR), SH does not always produce adequate results. For such cores, advanced homogenization techniques have been developed, such as Superhomogenization (SPH) [1] and Generalized Equivalence Theory (GET) [2]. Advanced homogenization techniques require additional homogenization parameters, besides the node-averaged multigroup macroscopic cross sections. SPH uses *SPH factors,* which are applied to each average macroscopic cross section in order to allow the corresponding node-integrated reaction rate for the homogenized node to exactly match the one for the heterogeneous node. GET employs *discontinuity factors* which change the flux continuity condition at node boundaries to a discontinuity condition, with the same goal of allowing

the node-integrated reaction rates for the homogenized node to match the ones of the heterogeneous node. At the interface ***s*** between two nodes i and j, the flux "discontinuity" condition is written

$$\overline{\Phi}_{sg}^{i} f_{sg}^{i} = \overline{\Phi}_{sg}^{j} f_{sg}^{j} \tag{1}$$

where $\overline{\Phi}_{sg}^{i}$ and $\overline{\Phi}_{sg}^{j}$ are the homogeneous fluxes on surface s in nodes i and j respectively, averaged over the common face. Factors f_{sg}^{i} and f_{sg}^{j} are called discontinuity factors, and are defined as the ratio of the face-averaged heterogeneous flux, $\overline{\Psi}$, to the face-averaged homogeneous flux, $\overline{\Phi}$:

$$f_{sg} \equiv \frac{\overline{\Psi}_{sg}}{\overline{\Phi}_{sg}} \tag{2}$$

The discontinuity of the face-averaged homogeneous flux expressed by equation (1) represents the continuity of the face-averaged heterogeneous flux across the interface.

While SPH can be used with any standard neutron diffusion code without requiring it to be changed (it merely requires the macroscopic cross sections to be scaled with the SPH factors), GET does require that the code be changed, to implement the discontinuity condition (1).

As mentioned, natural-uranium CANDU cores display only mild heterogeneity and hence do not usually require advanced homogenization methods. With the advent of the light-water-cooled and slightly-enriched-uranium-fuelled Advanced CANDU Reactor (ACR) this situation is expected to change. Some advanced homogenization method, be it GET or SPH is expected to be needed, and both methods' suitability for ACR cores will have to be investigated. Additionally, it may well turn out that improvements of even these advanced homogenization techniques will have to be considered. To allow such testing and experimentation to be performed at UOIT, it was considered desirable to develop a simple finite-difference diffusion code able to use GET via discontinuity factors. Such a code was deemed to also have didactical value for teaching students the principles of advanced homogenization methods and basic numerical methods. Consequently, the DISDIF3D code was created. In Canada, there exists to date only one other code combination able to use advanced homogenization methods: DRAGON-DONJON, developed at Ecole Polytechnique de Montréal [3], [4], [5]. The following sections present the finite-difference two-energy-group diffusion equations with discontinuity factors as implemented in DISDIF3D, together with the results of some preliminary testing of the new code.

2. Mesh-Centered Finite Differences with Discontinuity Factors

This section describes the mesh-centered finite-difference discretization of the multigroup diffusion equation when flux is assumed to be discontinuous on mesh boundaries. To do so, the domain is divided into parallelepipedic mesh boxes using a three-dimensional rectangular grid. Each mesh box is indexed with the triplet (i, j, k), where i, j, and k, correspond to directions x, y and z respectively. The side lengths of each mesh box are h_{xi}, h_{yj} and h_{zk}. A boundary between two meshes is denoted by a "½" in the index corresponding to the direction to which the boundary is

perpendicular. For example, the boundary between note (i,j,k) and node $(i,j+1,k)$ is denoted by $(i,j+1/2,k)$.

The grid planes perpendicular to the x axis intersect it at points x_i ($i=0,1,2,...$). The grid planes perpendicular to the y axis, intersect it at points y_j ($j=0,1,2,...$). The grid planes perpendicular to the z-axis intersect it at points z_k ($k=0,1,2,...$). It follows that

$$\begin{aligned} h_{xi} &= x_i - x_{i-1} \\ h_{yj} &= y_j - y_{j-1} \\ h_{zk} &= z_k - z_{k-1} \end{aligned} \tag{3}$$

It should be noted that the indexing of x, y and z axis points is somewhat inconsistent with the indexing of mesh boxes. Indeed, the consistent way of indexing these points would have been through the use of "1/2". For example, x_i would have been $x_{i+1/2}$ if the same indexing scheme as for the mesh boxes were used. Nonetheless, the integer indexing scheme has some advantages in terms of computer representation of the arrays x_i, y_j and z_k. With the current indexing scheme, x_i corresponds to the right limit of x mesh i. Analogous relations hold true for the y and z directions. This notation is illustrated for a two-dimensional situation, in Figure 1.

The mesh-centered finite-difference discretization method approximates the average flux in mesh (i,j,k), $\Phi_{i,j,k}$, by its value at the center of the box. According to Figure 1,

$$\Phi_{i,j,k} = \Phi\left(\frac{x_i + x_{i-1}}{2}, \frac{y_j + y_{j-1}}{2}, \frac{z_k + z_{k-1}}{2}\right) \tag{4}$$

The average values of the flux on mesh boundaries are approximated by the flux values at the midpoints of the boundaries, denoted by $\Phi_{i\pm1/2,j\pm1/2,k\pm1/2}$. For example, according to Figure 1,

$$\Phi_{i+1/2,j,k} = \Phi\left(x_i, \frac{y_j + y_{j-1}}{2}, \frac{z_k + z_{k-1}}{2}\right) \tag{5}$$

If the flux is discontinuous across a boundary, its (average) values on each side of the boundary can be indexed either with respect to the mesh to which they pertain or with respect to the boundary to which they refer. For example, the left value at the interface between mesh (i,j,k) and mesh $(i+1,j,k)$ can be denoted either by $\Phi^{x+}_{i,j,k}$ or by $\Phi^{x-}_{i+1/2,j,k}$. The first notation makes use of the fact that the value is to the right of the mesh (i,j,k), whereas the second notation makes use of the fact that the value is to the left of the boundary $(i+1/2,j,k)$. The two notations will be used interchangeably. Similar notations will be used for derivatives and other quantities.

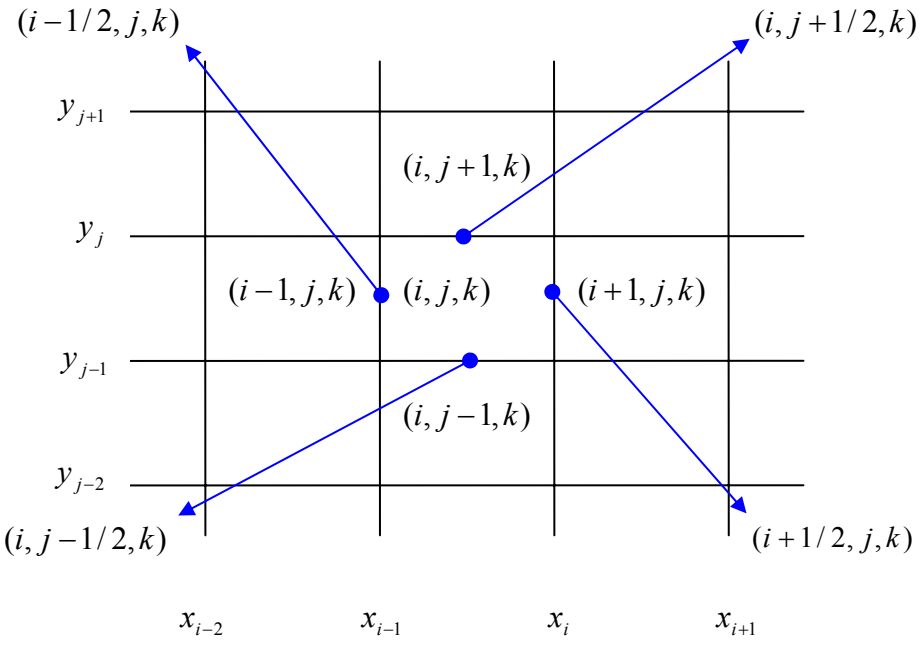

Figure 1 Mesh Indexing

Assuming the medium to be homogeneous within every mesh box (i,j,k), the two-group continuous diffusion equations for the (homogeneous) flux are written

$$\begin{aligned} -{}^1D\left(\frac{\partial^2({}^1\Phi)}{\partial x^2}+\frac{\partial^2({}^1\Phi)}{\partial y^2}+\frac{\partial^2({}^1\Phi)}{\partial z^2}\right)+{}^1\Sigma_r{}^1\Phi &= \frac{1}{k_{eff}}\left({}^1\nu\Sigma_f{}^1\Phi+{}^2\nu\Sigma_f{}^2\Phi\right) \\ -{}^2D\left(\frac{\partial^2({}^2\Phi)}{\partial x^2}+\frac{\partial^2({}^2\Phi)}{\partial y^2}+\frac{\partial^2({}^1\Phi)}{\partial z^2}\right)+{}^2\Sigma_a{}^2\Phi &= {}^{12}\Sigma_s{}^1\Phi \end{aligned} \tag{6}$$

where the left superscripts denote the energy group.

2.1 Interior Meshes

In what follows the finite differencing is illustrated for the x direction and then results are extended to the *y* and *z* direction. The group superscript is omitted, for clarity.

The backward-difference approximation of the left first derivative of the flux at the interface between nodes (i,j,k) and $(i+1,j,k)$ is written as

$$\left(\frac{\partial\Phi}{\partial x}\right)^{x-}_{i+1/2,j,k} \approx \frac{\Phi^{x+}_{i,j,k}-\Phi_{i,j,k}}{h_{xi}/2} \tag{7}$$

Similarly, the forward difference approximation to the right first derivative of the flux at the interface between nodes (i, j, k) and $(i+1, j, k)$ is written as

$$\left(\frac{\partial \Phi}{\partial x}\right)^{x+}_{i+1/2,j,k} \approx \frac{\Phi_{i+1,j,k} - \Phi^{x-}_{i+1,j,k}}{h_{xi+1}/2} \tag{8}$$

Note that in the above, the "+" and "–" signs are relative to the mesh for the fluxes and relative to the boundary for the derivatives.

The continuity of current and discontinuity of flux across boundaries can be used to express the boundary fluxes in terms of the center fluxes. First, the homogeneous-flux discontinuity across the mesh interface is applied.

$$f^{x+}_{i,j,k}\Phi^{x+}_{i,j,k} = f^{x-}_{i+1,j,k}\Phi^{x-}_{i+1,j,k} = \overline{\Psi}_{i+1/2,j,k} \tag{9}$$

It is to be noted that the heterogeneous flux, $\overline{\Psi}_{i+1/2,j,k}$, is continuous across the interface and hence it does not require references to its left and right values. Combining equation (9) with equations (7) and (8), the left and right derivatives at the interface can be expressed respectively as

$$\left(\frac{\partial \Phi}{\partial x}\right)^{-}_{i+1/2,j} \approx \frac{\dfrac{\overline{\Psi}_{i+1/2,j,k}}{f^{x+}_{i,j,k}} - \Phi_{i,j,k}}{h_{xi}/2} \tag{10}$$

$$\left(\frac{\partial \Phi}{\partial x}\right)^{+}_{i+1/2,j,k} \approx \frac{\Phi_{i+1,j,k} - \dfrac{\overline{\Psi}_{i+1/2,j,k}}{f^{x-}_{i+1,j,k}}}{h_{xi+1}/2} \tag{11}$$

The x-direction currents on the right and left of the interface are expressed as

$$\begin{aligned} J^{x-}_{i+1/2,j,k} &= -D_{i,j,k}\left(\frac{\partial \Phi}{\partial x}\right)^{x-}_{i+1/2,j,k} \\ J^{x+}_{i+1/2,j,k} &= -D_{i+1,j,k}\left(\frac{\partial \Phi}{\partial x}\right)^{x+}_{i+1/2,j,k} \end{aligned} \tag{12}$$

The continuity of current across the interface is thus written

$$\left(\frac{2D_{i,j,k}}{h_{xi}}\right)\left(\frac{\overline{\Psi}_{i+1/2,j,k}}{f^{x+}_{i,j,k}} - \Phi_{i,j,k}\right) = \left(\frac{2D_{i+1,j,k}}{h_{xi+1}}\right)\left(\Phi_{i+1,j,k} - \frac{\overline{\Psi}_{i+1/2,j,k}}{f^{x-}_{i+1,j,k}}\right) \tag{13}$$

Solving for the interface heterogeneous flux in the above yields

$$\overline{\Psi}_{i+1/2,j,k} = \frac{h_{xi+1} D_{i,j,k} \Phi_{i,j,k} + h_{xi} D_{i+1,j,k} \Phi_{i+1,j,k}}{\frac{h_{xi+1} D_{i,j,k}}{f^{x+}_{i,j,k}} + \frac{h_{xi} D_{i+1,j,k}}{f^{x-}_{i+1,j,k}}} \qquad (14)$$

Substituting equation (14) into equation (10) yields the derivative for the right boundary of mesh (i, j, k)

$$\left(\frac{\partial \Phi}{\partial x}\right)^{x-}_{i+1/2,j,k} = \frac{2D_{i+1,j,k}(f^{x-}_{i+1,j,k}\Phi_{i+1,j,k} - f^{x+}_{i,j,k}\Phi_{i,j,k})}{f^{x-}_{i+1,j,k} h_{xi+1,j,k} D_{i,j,k} + f^{x+}_{i,j,k} h_{xi,j,k} D_{i+1,j,k}} \qquad (15)$$

Following an argument similar to equations (7) to (16), the derivative at the left boundary of mesh (i, j, k) is

$$\left(\frac{\partial \Phi}{\partial x}\right)^{x+}_{i-1/2,j,k} = \frac{2D_{i-1,j,k}\left(f^{x-}_{i,j,k}\Phi_{i,j,k} - f^{x+}_{i-1,j,k}\Phi_{i-1,j,k}\right)}{f^{x-}_{i,j,k} h_{xi} D_{i-1,j,k} + f^{x+}_{i-1,j,k} h_{xi-1} D_{i,j,k}} \qquad (16)$$

Equations (15) and (16) can now be used to approximate the second-order x derivative for mesh (i, j, k)

$$\left(\frac{\partial^2 \Phi}{\partial x^2}\right)_{i,j,k} = \frac{1}{h_{xi}}\left[\left(\frac{\partial \Phi}{\partial x}\right)^{x-}_{i+1/2,j,k} - \left(\frac{\partial \Phi}{\partial x}\right)^{x+}_{i-1/2,j,k}\right] = \frac{1}{h_{xi}}\left[\frac{2D_{i+1,j,k}(f^{x-}_{i+1,j,k}\Phi_{i+1,j,k} - f^{x+}_{i,j,k}\Phi_{i,j,k})}{f^{x-}_{i+1,j,k} h_{xi+1,j,k} D_{i,j,k} + f^{x+}_{i,j,k} h_{xi,j,k} D_{i+1,j,k}} - \frac{2D_{i-1,j,k}\left(f^{x-}_{i,j,k}\Phi_{i,j,k} - f^{x+}_{i-1,j,k}\Phi_{i-1,j,k}\right)}{f^{x-}_{i,j,k} h_{xi} D_{i-1,j,k} + f^{x+}_{i-1,j,k} h_{xi-1} D_{i,j,k}}\right] \qquad (17)$$

To simplify notation, some new quantities are introduced

$$a^{x+}_{i,j,k} = \frac{-D_{i,j,k}}{h_{xi}} \frac{2f^{x-}_{i+1,j,k} D_{i+1,j,k}}{f^{x-}_{i+1,j,k} h_{xi+1} D_{i,j,k} + f^{x+}_{i,j,k} h_{xi} D_{i+1,j,k}} \qquad (18)$$

$$a^{cx+}_{i,j,k} = \frac{-D_{i,j,k}}{h_{xi}} \frac{2f^{x+}_{i,j,k} D_{i+1,j,k}}{f^{x-}_{i+1,j,k} h_{xi+1} D_{i,j,k} + f^{x+}_{i,j,k} h_{xi} D_{i+1,j,k}} \qquad (19)$$

$$a^{cx-}_{i,j,k} = \frac{-D_{i,j,k}}{h_{xi}} \frac{2f^{x-}_{i,j,k} D_{i-1,j,k}}{f^{x-}_{i,j,k} h_{xi} D_{i-1,j,k} + f^{x+}_{i-1,j,k} h_{xi-1} D_{i,j,k}} \qquad (20)$$

$$a^{x-}_{i,j,k} = \frac{-D_{i,j,k}}{h_{xi}} \frac{2f^{x+}_{i-1,j,k} D_{i-1,j,k}}{f^{x-}_{i,j,k} h_{xi} D_{i-1,j,k} + f^{x+}_{i-1,j,k} h_{xi-1} D_{i,j,k}} \qquad (21)$$

In terms of these new quantities, equation (17) is written

$$\left(\frac{\partial^2\Phi}{\partial x^2}\right)_{i,j,k} = \frac{-1}{D_{i,j,k}}\left[a^{x+}_{i,j,k}\Phi_{i+1,j,k} - (a^{cx+}_{i,j,k} + a^{cx-}_{i,j,k})\Phi_{i,j,k} + a^{x-}_{i,j,k}\Phi_{i-1,j,k}\right] \tag{22}$$

The superscripts on the above coefficients indicate to which boundary of the mesh they refer. Coefficients that multiply the current (central) mesh flux, (i,j,k), have a "c" superscript. Coefficients that multiply fluxes in neighboring meshes do not have the "c" superscript.

Relations similar to equation (22) can be derived for the *y* and *z*-directions.

$$\left(\frac{\partial^2\Phi}{\partial y^2}\right)_{i,j,k} = \frac{-1}{D_{i,j,k}}\left[a^{y+}_{i,j,k}\Phi_{i,j+1,k} - (a^{cy+}_{i,j,k} + a^{cy-}_{i,j,k})\Phi_{i,j,k} + a^{y-}_{i,j,k}\Phi_{i,j-1,k}\right] \tag{23}$$

$$\left(\frac{\partial^2\Phi}{\partial z^2}\right)_{i,j,k} = \frac{-1}{D_{i,j,k}}\left[a^{z+}_{i,j,k}\Phi_{i,j,k+1} - (a^{cz+}_{i,j,k} + a^{cz-}_{i,j,k})\Phi_{i,j,k} + a^{z-}_{i,j,k}\Phi_{i,j,k-1}\right] \tag{24}$$

Applying the finite-difference approximation outlined by equations (22) to (24) to the two-group diffusion equations (6), the following system of linear algebraic equations results

$$\begin{aligned}
&{}^1a^{x+}_{i,j,k}\,{}^1\Phi_{i+1,j,k} + {}^1a^{y+}_{i,j,k}\,{}^1\Phi_{i,j+1,k} + {}^1a^{z+}_{i,j,k}\,{}^1\Phi_{i,j,k+1} \\
&-\left({}^1a^{cx+}_{i,j,k} + {}^1a^{cy+}_{i,j,k} + {}^1a^{cz+}_{i,j,k} + {}^1a^{cx-}_{i,j,k} + {}^1a^{cy-}_{i,j,k} + {}^1a^{cz-}_{i,j,k}\right){}^1\Phi_{i,j,k} \\
&+{}^1a^{x-1}_{i,j,k}\,{}^1\Phi_{i-1,j,k} + {}^1a^{y-1}_{i,j,k}\,{}^1\Phi_{i,j-1,k} + {}^1a^{z-1}_{i,j,k-1}\,{}^1\Phi_{i,j,k} + \Sigma_{r1}\,{}^1\Phi_{i,j,k} \\
&= \frac{1}{k_{eff}}\left(\nu\Sigma_{f1}\,{}^1\Phi_{i,j,k} + \nu\Sigma_{f2}\,{}^2\Phi_{i,j,k}\right) \\
&{}^2a^{x+}_{i,j,k}\,{}^2\Phi_{i+1,j,k} + {}^2a^{y+}_{i,j,k}\,{}^2\Phi_{i,j+1,k} + {}^2a^{z+}_{i,j,k}\,{}^2\Phi_{i,j,k+1} \\
&-\left({}^2a^{cx+}_{i,j,k} + {}^2a^{cy+}_{i,j,k} + {}^2a^{cz+}_{i,j,k} + {}^2a^{cx-}_{i,j,k} + {}^2a^{cy-}_{i,j,k} + {}^2a^{cz-}_{i,j,k}\right){}^2\Phi_{i,j,k} \\
&+{}^2a^{x-}_{i,j,k}\,{}^2\Phi_{i-1,j,k} + {}^2a^{y-}_{i,j,k}\,{}^2\Phi_{i,j-1,k} + {}^2a^{z-}_{i,j,k}\,{}^2\Phi_{i,j,k-1} + \Sigma_{a2}\,{}^2\Phi_{i,j,k} \\
&= \Sigma_{12}\,{}^1\Phi_{i,j,k}
\end{aligned} \tag{25}$$

The following additional new quantities

$$\begin{aligned}
{}^1a^{c}_{i,j,k} &= -\left({}^1a^{cx+}_{i,j,k} + {}^1a^{cy+}_{i,j,k} + {}^1a^{cz+}_{i,j,k} + {}^1a^{cx-}_{i,j,k} + {}^1a^{cy-}_{i,j,k} + {}^1a^{cz-}_{i,j,k}\right) + \Sigma_{r1} \\
{}^2a^{c}_{i,j,k} &= -\left({}^2a^{cx+}_{i,j,k} + {}^2a^{cy+}_{i,j,k} + {}^2a^{cz+}_{i,j,k} + {}^2a^{cx-}_{i,j,k} + {}^2a^{cy-}_{i,j,k} + {}^2a^{cz-}_{i,j,k}\right) + \Sigma_{a2}
\end{aligned} \tag{26}$$

simplify the linear system to

$$
\begin{aligned}
&{}^{1}a^{x+}_{i,j,k}\,{}^{1}\Phi_{i+1,j,k} + {}^{1}a^{y+}_{i,j,k}\,{}^{1}\Phi_{i,j+1,k} + {}^{1}a^{z+}_{i,j,k}\,{}^{1}\Phi_{i,j,k+1} \\
&+ {}^{1}a^{x-}_{i,j,k}\,{}^{1}\Phi_{i-1,j,k} + {}^{1}a^{y-}_{i,j,k}\,{}^{1}\Phi_{i,j-1,k} + {}^{1}a^{z-}_{i,j,k}\,{}^{1}\Phi_{i,j,k-1} + {}^{1}a^{c}_{i,j,k}\,{}^{1}\Phi_{i,j,k} \\
&= \frac{1}{k_{eff}}\left(\nu\Sigma_{f1}\,{}^{1}\Phi_{i,j,k} + \nu\Sigma_{f2}\,{}^{2}\Phi_{i,j,k}\right) \\
&{}^{2}a^{x+}_{i,j,k}\,{}^{2}\Phi_{i+1,j,k} + {}^{2}a^{y+}_{i,j,k}\,{}^{2}\Phi_{i,j+1,k} + {}^{2}a^{z+}_{i,j,k}\,{}^{2}\Phi_{i,j,k+1} \\
&+ {}^{2}a^{x-}_{i,j,k}\,{}^{2}\Phi_{i-1,j,k} + {}^{2}a^{y-}_{i,j,k}\,{}^{2}\Phi_{i,j-1,k} + {}^{2}a^{z-}_{i,j,k}\,{}^{2}\Phi_{i,j,k-1} + {}^{2}a^{c}_{i,j,k}\,{}^{2}\Phi_{i,j,k} \\
&= \Sigma_{12}\,{}^{1}\Phi_{i,j,k}
\end{aligned}
\tag{27}
$$

2.2 External-Boundary Meshes

The linear systems (25) and (27) were derived for interior meshes. For boundary meshes different expressions for the coefficients have to be derived. The derivation will be presented only for the boundary perpendicular to the *x* axis and then extended to the *y* and *z* directions.

The formalism was implemented for homogeneous boundary conditions. To allow boundary conditions as general as possible to be simulated, mixed homogeneous boundary conditions were implemented by imposing the outward-current-to-flux ratio on each boundary

$$\gamma_{boundary} = \left(\frac{\vec{J}\hat{n}}{\Psi}\right)_{boundary} \tag{28}$$

where $\hat{n}$ is the unit normal to the outer boundary of the domain.

Mixed homogeneous boundary conditions allow great flexibility in simulating different boundary conditions. Through the choice of γ, reflective, zero-flux and vacuum boundary conditions can all be simulated. Vacuum boundary conditions can be transport-corrected or not. Additionally, artificial boundary conditions can be imposed at the limit of the fuel region, to simulate the presence of the reflector without actually modeling reflector meshes.

For an *x*-boundary node (b, j, k), the outward-current-to-flux ratio becomes

$$\gamma^{xu} = \frac{u\bar{J}^{x}_{b+u/2,j,k}}{\bar{\Psi}_{b+u/2,j,k}} = \frac{u\bar{J}^{xu}_{b,j,k}}{f^{xu}_{b,j,k}\Phi^{xu}_{b,j,k}} = \frac{u\bar{J}^{x(-u)}_{b+u/2,j,k}}{f^{xu}_{b,j,k}\Phi^{xu}_{b,j,k}} \tag{29}$$

In the above, "*u*" is the sign of the outward unit normal to the external boundary. It is -1 for the left boundary and +1 for the right boundary.

By applying the finite-differencing techniques to the boundary node, the derivative on the boundary is written as

$$\left(\frac{\partial\Phi}{\partial x}\right)^{x(-u)}_{b+u/2,j,k} = u\frac{\Phi^{xu}_{b,j,k} - \Phi_{b,j,k}}{h_{xb}/2} \tag{30}$$

The boundary current is written as

$$J^{x(-u)}_{b,j,k} = u\frac{-D_{b,j,k}\left(\Phi^{xu}_{b,j,k} - \Phi_{b,j,k}\right)}{h_{xb}/2} \tag{31}$$

The boundary condition is now written

$$\gamma^{xu} = \frac{-D_{b,j,k}\left(\Phi^{xu}_{b,j,k} - \Phi_{b,j,k}\right)}{\frac{h_{xb}}{2} f^{xu}_{b,j,k}\Phi^{xu}_{b,j,k}} \tag{32}$$

The boundary homogeneous flux is then written

$$\Phi^{x-}_{b,j,k} = \frac{2D_{b,j,k}\Phi_{b,j,k}}{h_{xb}\gamma^{x-}f^{x-}_{b,j,k} + 2D_{b,j,k}} \tag{33}$$

By substituting equation (33) into (30), the first derivative of the flux for the boundary becomes

$$\left(\frac{\partial\Phi}{\partial x}\right)^{xu}_{b+u/2,j,k} = \frac{\Phi_{b,j,k}}{\frac{D_{b,j,k}}{\gamma^{xu}f^{xu}_{b,j,k}} + \frac{h_{xb}}{2}} = \frac{-h_{xb}}{D_{b,j,k}} a^{cxu}_{b,j,k}\Phi_{b,j,k} \tag{34}$$

where $a^{cxu}_{b,j,k}$ is defined as

$$a^{cxu}_{b,j,k} = \frac{-1}{h_{xb}\left(\frac{1}{\gamma^{xu}f^{xu}_{b,j,k}} + \frac{h_{xb}}{2D_{b,j,k}}\right)} \tag{35}$$

The second-order *x*-partial derivative for a boundary mesh can now be expressed as

$$\left(\frac{\partial^2\Phi}{\partial x^2}\right)_{b,j,k} = -\frac{1}{D_{b,j,k}}\left[a^{x(-u)}_{b-u,j,k}\Phi_{b-u,j,k} - \left(a^{cx(-u)}_{b,j,k} + a^{cxu}_{b,j,k}\right)\Phi_{b,j,k}\right] \tag{36}$$

Equation (36) is the counterpart of equation (22) for boundary meshes. The differences reside in the absence of coefficient $a^{xu}_{b,j,k}$ and in the different expression for coefficient $a^{cxu}_{b,j,k}$. Coefficients $a^{x(-u)}_{b-u,j,k}$ and $a^{cx(-u)}_{b,j,k}$ are identical to those in equation (22).

Arguments similar to equations (29) to (36) apply for the *y* and *z* directions. The system (27) remains valid, with the mention that some coefficients need to be modified according to equation (35) (or its *y* or *z* counterparts) for boundary meshes. Overall, six boundary conditions need to be provided to the code: ($\gamma^{x-}, \gamma^{x+}, \gamma^{y-}, \gamma^{y+}, \gamma^{z-}, \gamma^{z+}$).

3. Numerical Solution of Eigenvalue-Eigenvector Problem

System (27) defines an eigenvalue-eigenvector problem

$$\underline{\underline{A}}\,\underline{\Phi} = \frac{1}{k_{eff}}\underline{\underline{F}}\,\underline{\Phi} \tag{37}$$

To find the maximum eigenvalue, k_{eff}, an inverse-power iteration is used. At each inverse-power iteration step, the system

$$\underline{\underline{A}}\,\underline{\Phi}^{n+1} = \frac{1}{k_{eff}}\underline{\underline{F}}\,\underline{\Phi}^{n} \tag{38}$$

is solved for $\underline{\Phi}^{n+1}$, using either a Successive Over-Relaxation (SOR) algorithm, or a Generalized Minimized Residual (GMRES) algorithm. The method of solution is user-selectable.

4. Preliminary Verification Results

A simple preliminary verification of DISDIF3D was performed using code-to-code comparison with NESTLE [6]. To verify that the code solves the two-group diffusion equation correctly, simple calculations were performed for a $10 \times 10 \times 12$ mesh parallelepiped and results were compared with those obtained with NESTLE. NESTLE was chosen because it can solve the diffusion equation by using either plain finite-differences (FD) without discontinuity factors or the Nodal Expansion Method (NEM) with discontinuity factors. Unfortunately, NESTLE does not provide the option of using FD with discontinuity factors. However, since the NEM is supposed to give results very close to the exact solution, i.e. a fine-mesh FD solution, good, if not perfect, agreement is to be expected between a fine-mesh FD solution with discontinuity factors and a NEM solution with discontinuity factors. While this latter approximate agreement does not offer perfect proof of the correctness of DISDIF3D, it offers some degree of confidence in it.

4.1 Test Models

The geometrical model used for comparison with NESTLE, consisted of a parallelepiped with $10 \times 10 \times 12$ nodes, 28.575 cm (11.25'') in the x and y directions and 49.53 cm (19.5'') in the z direction. Zero-flux boundary conditions were used. The material map was the same for all 12 *z* planes consisting of a checkerboard pattern of two materials, with properties detailed in Table 1.

	D_1	D_2	Σ_{a1}	Σ_{a2}	Σ_{12}	Σ_{21}	$\nu\Sigma_{f1}$	$\nu\Sigma_{f2}$	f_1	f_2
Material 1	1.31924	0.84417	0.00179	0.00393	0.00863	0.00000	0.00087	0.00475	0.80	1.10
Material 2	1.31924	0.84417	0.00179	0.00493	0.00863	0.00000	0.00087	0.00475	0.90	1.00

Table 1: Material Cross Sections and Discontinuity Factors

Calculations performed and comparisons made are detailed in Table 2.

	Calculation A	**Calculation B (reference)**
Comparison 1	**DISDIF3D** coarse-mesh FD (1x1x1) meshes/node no discontinuity factors	**NESTLE** coarse-mesh FD (1x1x1) meshes/node no discontinuity factors
Comparison 2	**DISDIF3D** fine-mesh FD (4x4x1) meshes/node no discontinuity factors	**NESTLE** NEM no discontinuity factors
Comparison 3	**DISDIF3D** fine-mesh FD (4x4x1) meshes/node discontinuity factors at node boundaries	**NESTLE** NEM discontinuity factors at node boundaries
Comparison 4	**NESTLE** NEM discontinuity factors at node boundaries	**NESTLE** NEM no discontinuity factors

Table 2: Calculations and Comparisons

The purpose of the first comparison was to verify that the FD method implemented in DISDIF3D produces the same results as the FD implemented in NESTLE, in the absence of discontinuity factors. The purpose of the second comparison was to verify that, as expected, fine mesh FD and NEM produce very similar results. The purpose of the third comparison, was to verify that the fine mesh FD method with discontinuity factors implemented in DISDIF3D produces close results to the NEM with discontinuity factors implemented in NESTLE, thus conferring some degree of confidence in the correctness of the implementation of discontinuity factors in DISDIF3D. Finally, the aim of the fourth comparison was to show that discontinuity factors introduce significant changes in the flux values, thus proving that comparison 3, between DISDIF3D and NESTLE results for the discontinuity-factor case, is meaningful and that it does not merely replicate comparison 2.

4.2 Test Results and Interpretation

It will be noted that, given the geometry of the model, the solution is separable in a function dependent only on *z* and a function dependent only on *x*, *y*, and energy.

$$\begin{bmatrix} {}^{1}\Phi_{i,j,k} \\ {}^{2}\Phi_{i,j,k} \end{bmatrix} = \varphi_k^z \begin{bmatrix} {}^{1}\varphi_{i,j}^{xy} \\ {}^{2}\varphi_{i,j}^{xy} \end{bmatrix} \tag{39}$$

It follows that instead of comparing the fluxes at all positions, it is sufficient to compare the normalized maps of ${}^{1}\varphi_{i,j}^{xy}$, ${}^{2}\varphi_{i,j}^{xy}$ and φ_k^z between calculation A and calculation B. Results for φ_k^z were found to be near-identical for all three comparisons, so only detailed comparisons between the normalized ${}^{1}\varphi_{i,j}^{xy}$, ${}^{2}\varphi_{i,j}^{xy}$ maps will be presented in what follows. The comparisons will be presented in the form of percent difference between results A and results B

$${}^{g}\varepsilon_{i,j} = \frac{\left({}^{g}\varphi_{i,j}^{xy}\right)_A - \left({}^{g}\varphi_{i,j}^{xy}\right)_B}{\left({}^{g}\varphi_{i,j}^{xy}\right)_B} \times 100 \tag{40}$$

The reference results for comparison 1 are presented in Table 3 and the differences in Table 4. The reference results for comparison 2 are presented in Table 5 and the differences in Table 6. The reference results for comparison 3 are presented in Table 7 and the differences in Table 8. Finally, the differences for comparison 4 are presented in Table 9.

It can be seen from Table 4 that the maximum percent difference is only 0.009% for the fast flux and 0.011% for the thermal flux. This means that the FD results obtained with DISDIF3D and with NESTLE are virtually identical, implying that the implementation of the FD equations without discontinuity factors in DISDIF3D is correct.

Table 6 shows that the maximum difference between the fine-mesh FD and nodal method, both without discontinuity factors, is 0.11% for the fast flux and 0.25% for the thermal flux. This is to be expected, as fine-mesh FD and NEM should give close but not identical results.

Table 8 shows maximum differences between the DISDIF3D and NESTLE results of 0.41% for the fast flux and 0.62% for the thermal flux. These values are comparable with, although somewhat larger than, those obtained in the absence of discontinuity factors which implies that discontinuity factors do not seem to induce large differences between DISDIF3D and NESTLE and hence they are likely implemented correctly.

Finally, the differences of 3%-5% that appear in Table 9 confirm that indeed the perturbation introduced by the discontinuity factors is significant and hence comparison 3 is, as desired, meaningful.

The simple preliminary verification that was described in this paper is not ideal. For one thing, it is a code-to-code comparison, so its validity depends on the correctness of the reference code. For another thing, the comparison for the discontinuity-factor methods was not entirely consistent, as FD and NEM were compared, thus differences being introduced. Additionally, there was no testing of different, arbitrary, geometries and material distributions. All these limitations will have to be

addressed in the future. Limitations of tests notwithstanding, the preliminary results indicate that DISDIF3D functions correctly.

5. Conclusion and Future Work

A new finite difference two-energy-group diffusion code, DISDIF3D, was created, which has the ability to use discontinuity factors. Preliminary tests indicate that the code functions correctly, but more extensive verification is required. Extension to a general multigroup formalism is desirable and should be pursued in the future.

keff	0.90224								
Gr 1 Flux									
0.0604	0.1716	0.2737	0.3368	0.3822	0.3733	0.3448	0.2672	0.1756	0.0591
0.1716	0.5158	0.7685	1.0116	1.0733	1.1213	0.9682	0.8026	0.4928	0.1756
0.2737	0.7685	1.2495	1.5094	1.7455	1.6732	1.5745	1.1978	0.8026	0.2672
0.3368	1.0116	1.5094	1.9844	2.1083	2.1997	1.9019	1.5745	0.9682	0.3448
0.3822	1.0733	1.7455	2.1083	2.4384	2.3372	2.1997	1.6732	1.1213	0.3733
0.3733	1.1213	1.6732	2.1997	2.3372	2.4384	2.1083	1.7455	1.0733	0.3822
0.3448	0.9682	1.5745	1.9019	2.1997	2.1083	1.9844	1.5094	1.0116	0.3368
0.2672	0.8026	1.1978	1.5745	1.6732	1.7455	1.5094	1.2495	0.7685	0.2737
0.1756	0.4928	0.8026	0.9682	1.1213	1.0733	1.0116	0.7685	0.5158	0.1716
0.0591	0.1756	0.2672	0.3448	0.3733	0.3822	0.3368	0.2737	0.1716	0.0604
Gr 2 Flux									
0.1149	0.3120	0.5215	0.6123	0.7283	0.6787	0.6570	0.4857	0.3345	0.1077
0.3120	0.9861	1.3929	1.9339	1.9454	2.1436	1.7547	1.5342	0.8930	0.3345
0.5215	1.3929	2.3885	2.7359	3.3365	3.0328	3.0099	2.1711	1.5342	0.4857
0.6123	1.9339	2.7359	3.7935	3.8214	4.2050	3.4472	3.0099	1.7547	0.6570
0.7283	1.9454	3.3365	3.8214	4.6614	4.2361	4.2050	3.0328	2.1436	0.6787
0.6787	2.1436	3.0328	4.2050	4.2361	4.6614	3.8214	3.3365	1.9454	0.7283
0.6570	1.7547	3.0099	3.4472	4.2050	3.8214	3.7935	2.7359	1.9339	0.6123
0.4857	1.5342	2.1711	3.0099	3.0328	3.3365	2.7359	2.3885	1.3929	0.5215
0.3345	0.8930	1.5342	1.7547	2.1436	1.9454	1.9339	1.3929	0.9861	0.3120
0.1077	0.3345	0.4857	0.6570	0.6787	0.7283	0.6123	0.5215	0.3120	0.1149

Table 3: Comparison 1 Reference Results

k-eff diff.	0.00000								
Gr 1 Flux % difference									
0.008%	0.004%	0.002%	-0.001%	-0.001%	0.002%	-0.002%	0.003%	0.005%	0.009%
0.004%	0.001%	0.001%	0.001%	0.000%	0.001%	-0.001%	0.000%	0.005%	0.005%
0.002%	0.001%	-0.001%	-0.001%	-0.001%	0.000%	0.000%	0.001%	0.000%	0.003%
-0.001%	0.001%	-0.001%	0.000%	-0.001%	-0.001%	-0.001%	0.000%	-0.001%	-0.002%
0.000%	0.000%	-0.001%	-0.001%	-0.001%	-0.001%	-0.001%	0.000%	0.002%	0.002%
0.002%	0.001%	0.000%	-0.001%	-0.001%	-0.001%	0.000%	-0.001%	0.000%	0.000%
-0.002%	-0.001%	0.000%	-0.001%	-0.001%	0.000%	0.000%	-0.001%	0.001%	0.000%
0.003%	0.000%	0.001%	0.000%	0.000%	-0.001%	-0.001%	0.000%	0.002%	0.003%
0.005%	0.005%	0.000%	-0.001%	0.001%	0.000%	0.001%	0.002%	0.001%	0.005%
0.009%	0.005%	0.003%	-0.002%	0.002%	0.000%	0.000%	0.003%	0.005%	0.009%
Gr 2 Flux % difference									
0.010%	0.006%	-0.002%	-0.002%	0.000%	-0.001%	0.000%	0.003%	0.004%	0.010%
0.006%	-0.001%	-0.002%	-0.003%	-0.003%	-0.002%	-0.002%	-0.001%	-0.002%	0.004%
-0.002%	-0.002%	-0.003%	-0.004%	-0.001%	-0.004%	-0.004%	-0.003%	-0.001%	0.003%
-0.002%	-0.003%	-0.004%	-0.007%	-0.002%	-0.005%	-0.004%	-0.004%	-0.002%	0.001%
0.000%	-0.003%	-0.001%	-0.002%	-0.006%	-0.001%	-0.004%	-0.004%	-0.002%	-0.001%
-0.001%	-0.002%	-0.004%	-0.005%	-0.001%	-0.006%	-0.002%	0.000%	-0.003%	0.000%
0.000%	-0.002%	-0.004%	-0.004%	-0.005%	-0.002%	-0.007%	-0.003%	-0.003%	-0.001%
0.003%	-0.001%	-0.003%	-0.004%	-0.004%	0.000%	-0.003%	-0.002%	-0.002%	-0.001%
0.004%	-0.002%	-0.001%	-0.002%	-0.002%	-0.003%	-0.003%	-0.002%	0.000%	0.007%
0.010%	0.004%	0.003%	0.001%	-0.001%	0.000%	-0.001%	-0.001%	0.007%	0.011%

Table 4: Comparison 1 Differences

keff	0.89891								
Gr 1 Flux									
0.0602	0.1734	0.2714	0.3402	0.3790	0.3771	0.3419	0.2699	0.1741	0.0595
0.1734	0.5067	0.7822	0.9942	1.0925	1.1020	0.9856	0.7889	0.5019	0.1741
0.2714	0.7822	1.2286	1.5356	1.7161	1.7022	1.5481	1.2186	0.7889	0.2699
0.3402	0.9942	1.5356	1.9507	2.1450	2.1624	1.9350	1.5481	0.9856	0.3419
0.3790	1.0925	1.7161	2.1450	2.3971	2.3778	2.1624	1.7022	1.1020	0.3771
0.3771	1.1020	1.7022	2.1624	2.3778	2.3971	2.1450	1.7161	1.0925	0.3790
0.3419	0.9856	1.5481	1.9350	2.1624	2.1450	1.9507	1.5356	0.9942	0.3402
0.2699	0.7889	1.2186	1.5481	1.7022	1.7161	1.5356	1.2286	0.7822	0.2714
0.1741	0.5019	0.7889	0.9856	1.1020	1.0925	0.9942	0.7822	0.5067	0.1734
0.0595	0.1741	0.2699	0.3419	0.3771	0.3790	0.3402	0.2714	0.1734	0.0602
Gr 2 Flux									
0.1130	0.3181	0.5094	0.6242	0.7114	0.6919	0.6417	0.4953	0.3269	0.1093
0.3181	0.9522	1.4338	1.8679	2.0028	2.0706	1.8067	1.4823	0.9199	0.3269
0.5094	1.4338	2.3078	2.8156	3.2234	3.1212	2.9080	2.2344	1.4823	0.4953
0.6242	1.8679	2.8156	3.6644	3.9329	4.0620	3.5478	2.9080	1.8067	0.6417
0.7114	2.0028	3.2234	3.9329	4.5027	4.3598	4.0620	3.1212	2.0706	0.6919
0.6919	2.0706	3.1212	4.0620	4.3598	4.5027	3.9329	3.2234	2.0028	0.7114
0.6417	1.8067	2.9080	3.5478	4.0620	3.9332	3.6644	2.8156	1.8679	0.6242
0.4953	1.4823	2.2344	2.9080	3.1212	3.2234	2.8156	2.3078	1.4338	0.5094
0.3269	0.9199	1.4823	1.8067	2.0706	2.0028	1.8679	1.4338	0.9522	0.3181
0.1093	0.3269	0.4953	0.6417	0.6919	0.7114	0.6242	0.5094	0.3181	0.1130

Table 5: Comparison 2 Reference Results

k-eff diff.	0.00021								
Gr 1 Flux % difference									
-0.10%	0.07%	-0.10%	0.07%	-0.09%	0.07%	-0.08%	0.09%	-0.08%	0.10%
0.07%	-0.03%	-0.02%	-0.01%	-0.02%	0.00%	-0.01%	0.01%	0.01%	-0.07%
-0.10%	-0.02%	0.01%	-0.05%	0.02%	-0.04%	0.03%	-0.03%	0.01%	0.09%
0.07%	-0.01%	-0.05%	0.02%	-0.04%	0.03%	-0.03%	0.03%	0.00%	-0.07%
-0.09%	-0.02%	0.02%	-0.04%	0.03%	-0.03%	0.03%	-0.03%	0.02%	0.09%
0.07%	0.00%	-0.04%	0.03%	-0.03%	0.03%	-0.03%	0.04%	0.00%	-0.07%
-0.08%	-0.01%	0.03%	-0.03%	0.03%	-0.03%	0.04%	-0.02%	0.02%	0.10%
0.09%	0.01%	-0.03%	0.03%	-0.03%	0.04%	-0.02%	0.04%	0.01%	-0.06%
-0.08%	0.01%	0.01%	0.00%	0.02%	0.00%	0.02%	0.01%	0.01%	0.11%
0.10%	-0.07%	0.09%	-0.07%	0.09%	-0.07%	0.10%	-0.06%	0.11%	-0.05%
Gr 2 Flux % difference									
-0.07%	0.02%	0.00%	0.00%	0.01%	0.01%	0.02%	0.02%	0.01%	0.12%
0.02%	0.14%	-0.18%	0.18%	-0.17%	0.19%	-0.16%	0.20%	-0.12%	0.01%
0.00%	-0.18%	0.22%	-0.22%	0.23%	-0.21%	0.24%	-0.20%	0.20%	0.03%
0.00%	0.18%	-0.22%	0.23%	-0.21%	0.24%	-0.20%	0.24%	-0.15%	0.04%
0.01%	-0.17%	0.23%	-0.21%	0.24%	-0.21%	0.24%	-0.20%	0.21%	0.03%
0.01%	0.19%	-0.21%	0.24%	-0.21%	0.24%	-0.20%	0.25%	-0.15%	0.04%
0.02%	-0.16%	0.24%	-0.20%	0.24%	-0.21%	0.25%	-0.19%	0.21%	0.03%
0.02%	0.20%	-0.20%	0.24%	-0.20%	0.25%	-0.19%	0.25%	-0.14%	0.04%
0.01%	-0.12%	0.20%	-0.15%	0.21%	-0.15%	0.21%	-0.14%	0.18%	0.06%
0.12%	0.01%	0.03%	0.04%	0.03%	0.04%	0.03%	0.04%	0.06%	-0.02%

Table 6: Comparison 2 Differences

keff	0.90315								
Gr 1 Flux									
0.0585	0.1783	0.2630	0.3500	0.3674	0.3880	0.3314	0.2777	0.1687	0.0610
0.1783	0.4907	0.8067	0.9629	1.1269	1.0674	1.0165	0.7640	0.5173	0.1687
0.2630	0.8067	1.1898	1.5848	1.6622	1.7569	1.4994	1.2574	0.7640	0.2777
0.3500	0.9629	1.5848	1.8896	2.2141	2.0948	1.9972	1.4994	1.0165	0.3314
0.3674	1.1269	1.6622	2.2141	2.3222	2.4545	2.0948	1.7569	1.0674	0.3880
0.3880	1.0674	1.7569	2.0948	2.4545	2.3222	2.2141	1.6622	1.1269	0.3674
0.3314	1.0165	1.4994	1.9972	2.0948	2.2141	1.8896	1.5848	0.9629	0.3500
0.2777	0.7640	1.2574	1.4994	1.7569	1.6622	1.5848	1.1898	0.8067	0.2630
0.1687	0.5173	0.7640	1.0165	1.0674	1.1269	0.9629	0.8067	0.4907	0.1783
0.0610	0.1687	0.2777	0.3314	0.3880	0.3674	0.3500	0.2630	0.1783	0.0585
Gr 2 Flux									
0.1180	0.3061	0.5316	0.6006	0.7426	0.6657	0.6698	0.4765	0.3409	0.1048
0.3061	1.0007	1.3718	1.9645	1.9164	2.1777	1.7286	1.5586	0.8801	0.3409
0.5316	1.3718	2.4285	2.6937	3.3927	2.9861	3.0606	2.1374	1.5586	0.4765
0.6006	1.9645	2.6937	3.8572	3.7634	4.2758	3.3948	3.0606	1.7286	0.6698
0.7426	1.9164	3.3927	3.7634	4.7403	4.1720	4.2758	2.9861	2.1777	0.6657
0.6657	2.1777	2.9861	4.2758	4.1720	4.7403	3.7634	3.3927	1.9164	0.7426
0.6698	1.7286	3.0606	3.3948	4.2758	3.7634	3.8572	2.6937	1.9645	0.6006
0.4765	1.5586	2.1374	3.0606	2.9861	3.3927	2.6937	2.4285	1.3718	0.5316
0.3409	0.8801	1.5586	1.7286	2.1777	1.9164	1.9645	1.3718	1.0007	0.3061
0.1048	0.3409	0.4765	0.6698	0.6657	0.7426	0.6006	0.5316	0.3061	0.1180

Table 7: Comparison 3 Reference Results

k-eff diff.	0.00006								
Gr 1 Flux % difference									
0.08%	-0.05%	0.17%	-0.09%	0.16%	-0.10%	0.17%	-0.08%	0.15%	0.05%
-0.05%	0.35%	-0.33%	0.37%	-0.34%	0.37%	-0.33%	0.37%	-0.27%	0.15%
0.17%	-0.33%	0.41%	-0.39%	0.40%	-0.40%	0.40%	-0.39%	0.38%	-0.08%
-0.09%	0.37%	-0.39%	0.40%	-0.40%	0.40%	-0.40%	0.41%	-0.33%	0.17%
0.16%	-0.34%	0.40%	-0.40%	0.40%	-0.41%	0.40%	-0.40%	0.37%	-0.10%
-0.10%	0.37%	-0.40%	0.40%	-0.41%	0.40%	-0.40%	0.40%	-0.33%	0.17%
0.17%	-0.33%	0.40%	-0.40%	0.40%	-0.40%	0.40%	-0.39%	0.37%	-0.08%
-0.08%	0.37%	-0.39%	0.41%	-0.40%	0.40%	-0.39%	0.41%	-0.32%	0.17%
0.15%	-0.27%	0.38%	-0.33%	0.37%	-0.33%	0.37%	-0.32%	0.35%	-0.04%
0.05%	0.15%	-0.08%	0.17%	-0.10%	0.17%	-0.08%	0.17%	-0.05%	0.08%
Gr 2 Flux % difference									
0.03%	0.30%	0.36%	0.27%	0.35%	0.27%	0.35%	0.27%	0.36%	0.62%
0.30%	0.38%	0.26%	0.35%	0.25%	0.35%	0.25%	0.35%	0.26%	0.36%
0.36%	0.26%	0.34%	0.25%	0.33%	0.24%	0.33%	0.25%	0.36%	0.27%
0.27%	0.35%	0.25%	0.32%	0.24%	0.32%	0.24%	0.33%	0.25%	0.35%
0.35%	0.25%	0.33%	0.24%	0.32%	0.24%	0.32%	0.24%	0.35%	0.27%
0.27%	0.35%	0.24%	0.32%	0.24%	0.32%	0.24%	0.33%	0.25%	0.35%
0.35%	0.25%	0.33%	0.24%	0.32%	0.24%	0.32%	0.25%	0.35%	0.27%
0.27%	0.35%	0.25%	0.33%	0.24%	0.33%	0.25%	0.34%	0.26%	0.37%
0.36%	0.26%	0.36%	0.25%	0.35%	0.25%	0.35%	0.26%	0.38%	0.31%
0.62%	0.36%	0.27%	0.35%	0.27%	0.35%	0.27%	0.37%	0.31%	0.03%

Table 8: Comparison 3 Differences

k-eff diff.	0.00424								
Gr 1 Flux % difference									
-2.79%	2.85%	-3.08%	2.88%	-3.07%	2.89%	-3.08%	2.86%	-3.12%	2.37%
2.85%	-3.15%	3.13%	-3.15%	3.14%	-3.14%	3.14%	-3.16%	3.05%	-3.12%
-3.08%	3.13%	-3.16%	3.20%	-3.14%	3.21%	-3.15%	3.19%	-3.16%	2.86%
2.88%	-3.15%	3.20%	-3.13%	3.22%	-3.13%	3.21%	-3.15%	3.14%	-3.08%
-3.07%	3.14%	-3.14%	3.22%	-3.12%	3.23%	-3.13%	3.21%	-3.14%	2.89%
2.89%	-3.14%	3.21%	-3.13%	3.23%	-3.12%	3.22%	-3.14%	3.14%	-3.07%
-3.08%	3.14%	-3.15%	3.21%	-3.13%	3.22%	-3.13%	3.20%	-3.15%	2.88%
2.86%	-3.16%	3.19%	-3.15%	3.21%	-3.14%	3.20%	-3.16%	3.13%	-3.08%
-3.12%	3.05%	-3.16%	3.14%	-3.14%	3.14%	-3.15%	3.13%	-3.15%	2.85%
2.37%	-3.12%	2.86%	-3.08%	2.89%	-3.07%	2.88%	-3.08%	2.85%	-2.79%
Gr 2 Flux % difference									
4.50%	-3.79%	4.37%	-3.79%	4.39%	-3.79%	4.38%	-3.80%	4.30%	-4.09%
-3.79%	5.09%	-4.33%	5.17%	-4.31%	5.17%	-4.32%	5.15%	-4.33%	4.30%
4.37%	-4.33%	5.23%	-4.33%	5.25%	-4.33%	5.25%	-4.34%	5.15%	-3.80%
-3.79%	5.17%	-4.33%	5.26%	-4.31%	5.26%	-4.31%	5.25%	-4.32%	4.38%
4.39%	-4.31%	5.25%	-4.31%	5.28%	-4.31%	5.26%	-4.33%	5.17%	-3.79%
-3.79%	5.17%	-4.33%	5.26%	-4.31%	5.28%	-4.31%	5.25%	-4.31%	4.39%
4.38%	-4.32%	5.25%	-4.31%	5.26%	-4.32%	5.26%	-4.33%	5.17%	-3.79%
-3.80%	5.15%	-4.34%	5.25%	-4.33%	5.25%	-4.33%	5.23%	-4.33%	4.37%
4.30%	-4.33%	5.15%	-4.32%	5.17%	-4.31%	5.17%	-4.33%	5.09%	-3.79%
-4.09%	4.30%	-3.80%	4.38%	-3.79%	4.39%	-3.79%	4.37%	-3.79%	4.50%

Table 9: Comparison 4 Differences

6. References

[1] Hébert A., “A Consistent Technique for Pin-by-Pin Homogenization of a Pressurized Water Reactor Assembly”, Nucl. Sci. Eng. Vol. 113, 1993, pp. 227-238

[2] Smith K., “Spatial Homogenization Methods for Light Water Reactor Analysis,” Ph.D. thesis, MIT, 1980

[3] Marleau G., Hebert A. and Roy R., "A User Guide for DRAGON 3.05", Institut de génie nucléaire, Departement de génie physique, Ecole Polytechnique de Montréal, 2006

[4] Varin E., Hebert A., Roy R. and Koclas J., “A User Guide for DONJON, Version 3.01”, Institut de génie nucléaire, Departement de génie physique, Ecole Polytechnique de Montréal, 2005

[5] P. Dufour, “Implantation de la theorie d’equivalence dans la chaıne de calcul DRAGON/DONJON-NDF”, Master thesis, Ecole Polytechnique de Montréal, Institut de génie nucléaire, 2004

[6] Turinsky P. J. et al., "NESTLE (V5.2.1) Few-Group Neutron Diffusion Equation Solver Utilizing The Nodal Expansion Method for Eigenvalue, Adjoint, Fixed-Source Steady-State and Transient Problems", Electric Power Research Center, North Carolina State University, Raleigh NC, 2003